RESEARCH ARTICLE

Key Points:
- BSO heat transport controls Barents Sea ice cover in terms of congelation growth
- Bottom melting controls sea ice mass variability in the Central Arctic Ocean
- Ocean has stronger direct impact on changes in sea ice mass than the atmosphere

Correspondence to:
A. B. Sandø,
anne.britt.sando@imr.no

Poleward ocean heat transports, sea ice processes, and Arctic sea ice variability in NorESM1-M simulations

A. B. Sandø[1,3], Y. Gao[2,3,4], and H. R. Langehaug[2,3]

[1]Institute of Marine Research, Bergen, Norway, [2]Nansen Environmental and Remote Sensing Center, Bergen, Norway, [3]Bjerknes Centre for Climate Research, Bergen, Norway, [4]Nansen-Zhu International Research Center, Institute of Atmospheric Physics, Beijing, China

Abstract Results from the NorESM1-M coupled climate model were used to examine relationships between Arctic sea ice area and ocean heat transports through the primary Arctic gateways. Comparisons were made with two other models (CNRM-CM5 and MRI-CGM3) that are part of the CMIP5 archive which have the required outputs for calculating ocean heat transports. Based on an evaluation, NorESM1-M was found to be best suited to study the effects of heat transports on sea ice area, and conclusions are based on results from this model. The Arctic Ocean was divided into two regions, the Barents Sea and the Central Arctic Ocean. The sea ice area variability was further analyzed in terms of frazil and congelation growth, top and bottom melting, and heat transports in the Barents Sea Opening (BSO) and the Fram Strait (FS). In the Barents Sea, increased heat transport in the BSO has a strong influence on sea ice area in terms of reduced congelation growth, while bottom melting is important for the variability in the Central Arctic Ocean. The negative trend in sea ice area is considerably greater in the Barents Sea than in the Central Arctic Ocean, despite the Central Arctic Ocean area being much larger, and reflects the major trend in the BSO heat transport. The model results in this study suggest that the ocean has stronger direct impact on changes in sea ice mass in terms of freezing and melting than the atmosphere, both in the mean and with respect to variability.

1. Introduction

The loss in Arctic sea ice has been attributed both to anthropogenic forcing and natural variability [*Lindsay and Zhang*, 2005; *Serreze and Francis*, 2006; *Kay et al.*, 2011], and numerous efforts have been made to find the dominant effect. Most studies conclude that both internal and external forcings are needed to explain the variability in sea ice area, but that the recent reduction is strongly related to global warming and human influence [*Serreze et al.*, 2007; *Min et al.*, 2008; *Polyakov et al.*, 2010; *Bekryaev et al.*, 2010; *Comiso*, 2012].

Most of the climate models that participated in the third phase of the Coupled Model Intercomparison Project (CMIP3) and the Intergovernmental Panel on Climate Change Fourth Assessment Report (IPCC AR4) underestimate the observed September trend [*Stroeve et al.*, 2007; *Boé et al.*, 2009], and there are large uncertainties in the projections of the Arctic sea ice area evolution [*IPCC*, 2007]. September trends calculated from models contributing to CMIP5 are more consistent with observations over the satellite era (1979–2011) [*Stroeve et al.*, 2012]. Nevertheless, the spread in projected CMIP5 September sea ice area throughout the 21st century is just as large as in the CMIP3 simulations, and the uncertainty as to when the Arctic Ocean will be seasonally ice-free remains large. Understanding the governing processes behind sea ice variability and trends is therefore of great importance for improving projections of future sea ice area.

The Arctic sea ice area variability reflects changes in poleward ocean heat transports [*Helland-Hansen and Nansen*, 1909; *Ingvaldsen et al.*, 2002; *Sandø et al.*, 2010], atmosphere-ocean heat fluxes [*Smedsrud et al.*, 2010], ice-albedo [*Lindsay and Zhang*, 2005], atmospheric circulation [*Overland et al.*, 2008], and ice export through the Fram Strait [*Langehaug et al.*, 2013]. These processes may in turn strongly affect the projections through feedback mechanisms in climate models [*Smedsrud et al.*, 2013]. Cause and effect is therefore not straightforward since they have mutual influence. Northward shifts of the Polar Front and corresponding
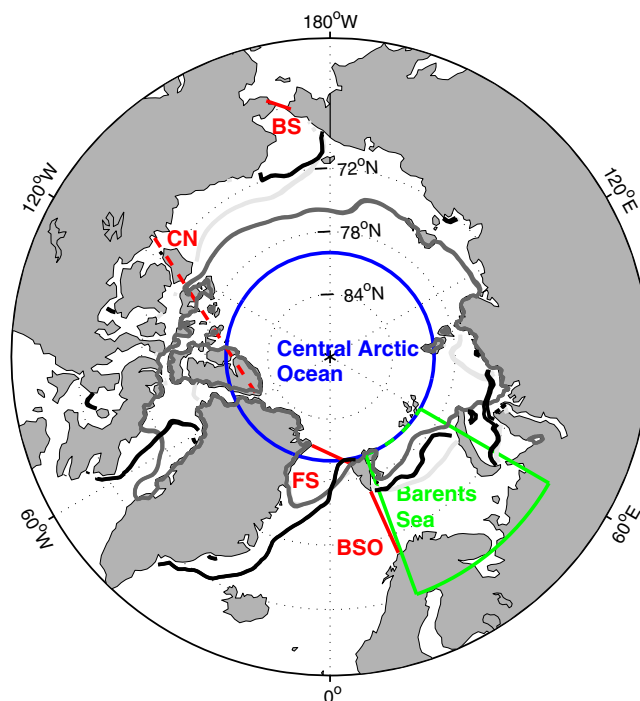
Figure 1. Gateways into the Arctic region (red), and boundaries for the two different areas investigated in this study: Barents Sea (green) and Central Arctic Ocean (blue). The gateways are the Bering Strait (BS), the Barents Sea Opening (BSO), the Canadian Archipelago and Nares Strait (CN), and the Fram Strait (FS). Contours are mean sea ice cover in September (1950–2005) for CNRM-CM5 (light gray), MRI-CGCM3 (gray), and NorESM1-M (black) where sea ice concentration is equal to 15%.

shifts in the winter ice edge may affect the location and extent of areas with strong heat loss, and increased ocean heat transport can therefore be compensated by cooling in these areas [*Smedsrud et al.*, 2010]. Alternatively, the strength of the Atlantic inflow reflects the changes in the northern heat loss [*Eldevik and Nilsen*, 2013]. Numerous examples of how different atmospheric patterns and associated geostrophic winds correspond to temperature and sea ice anomalies, sea ice advection, and increased ocean heat are discussed by *Overland et al.* [2008]. *Lindsay and Zhang* [2005] hypothesize that gradually increasing air temperatures through the last 50 years in tandem with shifts in atmospheric circulation have led to reduced thickness of first-year ice and flushing of thicker ice out of the Arctic basin, increasingly open summer water, and increasing absorption of solar radiation, melting the ice, warming the water, and promoting further thinning of first-year ice.

In this study, we investigate further the relationship between poleward ocean heat transports and sea ice area (sea ice concentration >0), and quantify contributions from different freezing and melting processes to sea ice area variability. Figure 1 shows an overview of the Arctic region and the corresponding gateways. Three different coupled climate models are evaluated with respect to mean ocean heat transport in these gateways and to seasonal variability in the Barents Sea Opening (BSO). BSO heat transport is also particularly important to evaluate due to its high contribution to poleward heat transport (Table 1). Based on this evaluation, the corresponding model ensemble is chosen to study the variability of the sea ice area in terms of different types of freezing and melting, and ocean heat transport.

Table 1. Estimates of Poleward Heat Transports (TW) From Studies Based on Observations, and From Model Results in the Bering Strait (BS), the Barents Sea Opening (BSO), the Canadian Archipelago and Nares Strait (CN), and the Fram Strait (FS)[a]

	BSO	BS	CN	FS
Aagaard and Greisman [1975]		3.8 (−0.1)	5.3 (−0.1)	67.2 (−0.1)
Curry et al. [2011]			20 ± 9 (0)	
Cuny et al. [2005]			18 ± 17 (0)	
Harms et al. [2005][*]	73 (0)			
Hopkins [1991]		3.8 (−0.1)	5.3 (−0.1)	47.5(−0.1)
Maslowski et al. [2004][*]	78 ± 15 (−0.1)			10 ± 9 (−0.1)
Mosby [1962]		11.1 (−0.1)	7.8 (−0.1)	31.9 (−0.1)
Rudels [1987]		3.1 (−0.1)	3.1 (−0.1)	18 (−0.1)
Sandø et al. [2010]*	74 (0)			
Smedsrud et al. [2010]	70 (0)			
Tsubouchi et al. [2012]	103 (0)		11 (−0.1)	
Zhang and Zhang [2001]*		7.7 (−0.1)	−1.3 (−0.1)	14.3 (−0.1)
Vowinkel and Orvig [1970]		3.8 (−0.1)	0.1 (−0.1)	27 (−0.1)
Mean of observation and simulation based est.	79.6 ± 13.4	5.6 ± 3.2	7.7 ± 7.4	30.8 ± 20.4

[a]Estimates from model results are indicated by an asterisk. The numbers in brackets are the relative temperatures used to calculate heat transports described in section 3.

Table 2. Modeled Ensemble Mean Heat Transports (TW) Into the Arctic Ocean Relative to a Reference Temperature of 0°C in the Four Gateways listed in Table 1 in the Bering Strait (BS), the Barents Sea Opening (BSO), the Canadian Archipelago and Nares Strait (CN), and the Fram Strait (FS)[a]

	BSO	BS	CN	FS
CNRM-CM5	43.1 ± 15	6.7 ± 19	4.9 ± 1	12.8 ± 1
MRI-CGCM3	47.4 ± 16	2.8 ± 4	2.1 ± 1	9.3 ± 4
NorESM1-M	53.6 ± 13	2.5 ± 4	11.8 ± 2	35.6 ± 8

[a]The model output are provided by the following modeling groups: The Centre National de Recherches Météorologiques/Centre Européen de Recherche et Formation Avancée en Calcul Scientifique (CNRM-CM5), the Japanese model from the Meteorological Research Institute (MRI-CGCM3), and the Norwegian model from the Norwegian Climate Center (NorESM1-M).

The coupled climate models are introduced in section 2, and evaluated in section 3. Methods used in the statistical analysis are described in section 4, while the results are presented and discussed in sections 5 and 6, respectively. Concluding remarks are given in section 7.

2. Climate Models and Simulations

The model results are drawn from the CMIP5 archive [*Taylor et al.*, 2012], which provides a range of distinct experiments from different coupled climate and earth system models. The purpose of these experiments is to address scientific questions that arose as part of the IPCC AR4 process, to improve the understanding of climate, and to get estimates of future change. To investigate the relationship between the ocean heat transport, sea ice processes, and Arctic sea ice area variability in the recent past and present climate, the historical experiment (1850–2005) is used. Unless otherwise specified, the results in this study are based on the period 1950–2005. These years were chosen because most observations were available from this period. A similar analysis was made for the years 1850–1905, but conclusions on variability did not differ from the ones presented for the later period.

The output needed to calculate ocean heat transports through specified sections based on accumulated heat transports from each time step were only available from three models. These variables, hfx and hfy, give the vertically integrated heat transport at each grid point, and transports in different sections are found by summing these components along zig-zag paths corresponding to these specified sections. Here three ensemble members from these three different models were used, namely the French model from the Centre National de Recherches Météorologiques/Centre Européen de Recherche et Formation Avancée en Calcul Scientifique (CNRM-CM5) [*Voldoire et al.*, 2011], the Japanese model from the Meteorological Research Institute (MRI-CGCM3) [*Yukimoto et al.*, 2012], and the Norwegian model from the Norwegian Climate Center (NorESM1-M) [*Bentsen et al.*, [2013]. The seasonal cycle, interannual variance, and long-term trends of sea ice properties such as area and ice export in these models were assessed by *Langehaug et al.* [2013]. They found that all models had a fully ice covered Arctic Ocean in March for the period 1979–2005. NorESM1-M simulated a realistic mean sea ice area for this month, whereas MRI-CGCM3 and CNRM-CM5 had ice extending too far south in the Atlantic and Pacific sectors, respectively. The selected models also had too much September sea ice in many regions in the Atlantic sector. NorESM1-M was the model with the largest overestimate in September [*Langehaug et al.*, 2013], as also indicated by Figure 1.

3. Observations and Model Evaluations

3.1. Mean Ocean Heat Transport

Estimates from the literature on poleward ocean heat transports through the four gateways into the Arctic are listed in Table 1. The numbers are a collection of calculations based on observations only, pure model estimates, or results from an inverse model to observations, where model results are marked with an asterisk. The reference temperature in the heat transport calculations differs from study to study. For easy comparisons with the simulated heat transports in this study, only estimates with a reference temperature close to 0°C are included in Table 1. Table 2 lists the simulated heat transports from the models used in this study, where the numbers represent the ensemble mean and standard deviation for each model.

In the BSO, current meter moorings have been operated since September 1997 [*Ingvaldsen et al.*, 2004]. These moorings, which were deployed every 30 nautical miles from 71°30′N to 73°30′N with instruments

measuring current velocity and temperature between 50 m depth and 15 m above bottom, allow for calculations of Atlantic Water (AW) volume and heat transports through the BSO. Heat transports provided by the CMIP5 models are net transports which involve inflows and outflows of different water types. Transports in BSO consist of warm AW with salinity above 35 and temperature above 3°C, relatively fresh inflow via the Norwegian Coastal Current with salinity below 34.7 and temperature above 3°C [*Loeng*, 1991; *Skagseth et al.*, 2008], and cold outflow in the Bear Island Trough with salinity around 35 and temperature around 2°C [*Skagseth*, 2008]. All these water mass types should therefore be taken into account when evaluating the BSO transports. The mean poleward heat transport by AW in BSO from 1997–2007 was calculated to be 48 TW [*Skagseth et al.*, 2008], while a combination of a 1 year full depth current meter profile in the core of the Norwegian Coastal Current and repeated hydrographic profiles yielded a heat transport of 34 TW [*Skagseth et al.*, 2011]. The estimated heat transport associated with the outflow, which is mainly recirculated AW in the Bear Island Trough, is 12 TW [*Skagseth*, 2008]. This leads to a net inflow of 70 TW [*Smedsrud et al.*, 2010] and is in good agreement with model estimates of *Maslowski et al.* [2004] (78 TW), *Harms et al.* [2005] (73 TW), and *Sandø et al.* [2010] (74 TW) (Table 1). *Tsubouchi et al.* [2012] used an inverse model and hydrographic observations from summer 2005 to estimate quasisynoptic net fluxes of volume, heat, and freshwater in gateways into the Arctic and arrived at a considerably larger estimate of 103 TW, mainly due to their 1.5 Sv larger inflow in the central BSO. *Skagseth et al.* [2008] found a trend of 2.5 TW per year (1997–2006), and *Årthun et al.* [2012] showed large interannual variability in the AW heat transport from 1997 to 2010 with anomalies exceeding ±20 TW, which may partly explain the large estimate by *Tsubouchi et al.* [2012] in 2005.

Ensemble mean BSO ocean heat transports from the different models in this study are shown in Table 2. NorESM1-M has the mean value closest to observations. All selected models underestimate the observed BSO heat transport, and this was also a problem in some of the CMIP3 models which in turn simulated overly extensive sea ice cover in the Barents Sea [*Melsom et al.*, 2009; *Sandø et al.* 2014].

Compared to the mean in Table 1, CNRM-CM5 is closest in the Bering Strait (BS), but all models in this study are within the range.

This is also the case for the Canadian Archipelago and Nares Strait (CN), where Table 1 shows large spread between the estimates, but NorESM1-M is closest to the most recent estimates.

In the Fram Strait (FS), estimates of mean AW heat transport (higher than 1°) vary strongly from 26 TW in 1998 to almost 50 TW in 2004 [*Schauer et al.*, 2008], consistent with the strong BSO variability as described by *Årthun et al.* [2012]. This strong variability might be the reason for the large spread in the estimates given in Table 1. The model results in Table 2 also show large spread, but all estimates are within the range of the observation and simulation based mean estimate. As in the BSO, NorESM1-M is closest to the mean.

3.2. Seasonal Cycle of Ocean Heat Transport

While the simulations used here incorporate best estimates of historical climate change forcings, simulated and observed time series of weather events and computed indices of atmospheric teleconnection patterns (such as the North Atlantic Oscillation) will be essentially uncorrelated. To evaluate the models against observed times series of BSO heat transport, focus is here on the skill of the model to reproduce seasonal timing such as maximum and minimum of the heat transport, the variance of the heat transport, and the root mean square (RMS) difference between the simulated and observed heat transport. A Taylor diagram [*Taylor*, 2001] is used to plot these properties for each model ensemble member (Figure 2). From this it can be concluded that CNRM-CM5 and NorESM1-M, where ensembles are close to each other, reproduce the BSO seasonal cycle better than MRI-CGCM3, both with respect to correlation and RMS. In addition, the above evaluation of the mean transports shows that NorESM1-M is closest to observations both in the BSO and the FS (Table 1). In the mean state, BSO and FS heat transports contribute most to the net poleward heat transport into the Arctic Ocean (Table 1), and the variability in these heat transports are important for the Barents Sea and Arctic sea ice extent [*Sandø et al.*, 2010; *Årthun et al.*, 2012; *Ivanov et al.*, 2012]. Based on this, NorESM1-M is found to be more suitable to study the effects of heat transports on the sea ice area than MRI-CGCM3 and CNRM-CM5. Furthermore, NorESM1-M is closest to the observed seasonal cycle and interannual variance of the Arctic sea ice cover [*Langehaug et al.*, 2013].
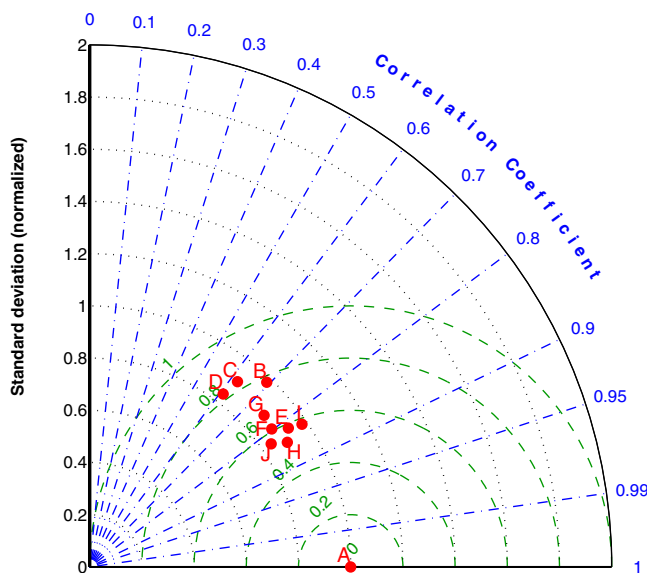
Figure 2. Taylor plot showing standard deviation (black), correlation coefficients (blue), and centered root mean square (RMS, green) difference between simulated and observed Barents Sea Opening heat transport [*Ingvaldsen et al.*, 2004]. The model time series are from the three first ensembles of MRI-CGCM3 (B, C, D), NorESM1-M (E, F, G), and CNRM-CM5 (H, I, J).

4. Methods

To study the implications of ocean heat transport on sea ice variability, we make use of a suite of variables available from the CMIP5 archive involving top and bottom melting, and ice growth due to congelation and frazil sea ice formation. In nature, frazil ice is made of small needle-like ice crystals which form as ocean water begins to freeze. Sheets of ice can form when frazil ice crystals float to the surface and accumulate. Depending on the weather conditions, sheets of ice form from grease ice or pancake ice. Finally, the sheet thickens into a more stable sheet of ice with a smooth surface below, called congelation ice. Only congelation ice can develop below the sheet of ice since frazil ice cannot form in the relatively still waters below the ice. These processes are described in detail in *Hunke and Lipscomb* [2010].

Frazil ice forms when the ocean temperature drops below its freezing temperature, which is a function of sea water salinity. Melting at the surface is a function of the surface temperature (i.e., the temperature of ice or snow at the interface with the atmosphere) and the net energy flux from the atmosphere to the ice (i.e., sensible heat flux, latent heat flux, incoming longwave flux, outgoing longwave flux, incoming shortwave flux, albedo, and fraction of absorbed shortwave flux that penetrates into the ice). The albedo can be altered by the presence of melt ponds [*Hunke and Lipscomb*, 2010]. Growth and melting at the bottom ice interface are functions of the conductive heat flux through the ice and the vertical ocean heat flux supplied to the bottom of the ice. The conductive heat at the bottom surface is dependent on the thermal conductivity of sea ice, the temperature gradient in the sea ice, and the freezing temperature, while the vertical heat flux from the ocean to the ice is mainly a function of the mixed layer temperature. The equations for the thermodynamics briefly described here can be found in *Hunke and Lipscomb* [2010].

The relationships between ocean heat transport, vertical air-sea heat flux, and sea ice area can be studied in detail by investigating correlations and trends of deseasoned time series. For this purpose, the Arctic has here been divided into two sectors: The Barents Sea and Central Arctic Ocean (Figure 1). The area named Central Arctic Ocean is the part north of 80°N which is more or less permanently covered by sea ice. The Barents Sea has a more seasonal ice cover, and is here restricted by the area between 66°N and 80°N and 20°E and 60°E. For each time step, variables are summed for ice covered grid cells only (i.e., sea ice concentration >0). To investigate possible relationships, hypotheses are tested by correlating these time series. Correlations are done on monthly time series which are deseasoned by detrending of each calendar month separately. The effective degrees of freedom are found according to *Chelton* [1983], i.e., taking into consideration the autocovariance and crosscovariance of the two time series. Significance levels are calculated by the standard Student's *t* test, using $\alpha = 0.05$ (5% significance level). Trends are calculated by the method described in *Santer et al.* [2008]. In addition, horizontal correlations plots are also presented to study the spatial variations.

The monthly time series contain some noise which drastically reduces the correlation values compared to annual time series. While monthly time series are chosen in this analysis in order to study the time lags in the correlation on these time scales, it should be kept in mind that more variability can be explained by using filtered time series.

Table 3. Annual Means (kg s^{-1}), Trends (kg s^{-1}), and Relative Trends (−) of Change in Sea Ice Mass Due to Different Processes in the Barents Sea and Central Arctic Ocean[a]

	Barents Sea			Central Arctic Ocean		
	Mean	Trend	Rel. trend	Mean	Trend	Rel. trend
Bottom melting	3.2e+07	−4.6e03	−1.4e−04	4.3e+07	1.1e04	2.5e−04
Top melting	1.4e+06	−5.7e02	−4.2e−04	7.4e+05	1.2e03	1.6e−03
Congelation growth	2.4e+07	−1.0e04	−4.2e−04	9.2e+07	4.2e03	4.6e−05
Frazil growth	8.3e+06	−2.7e03	−3.3e−04	1.5e+07	1.4e02	9.2e−06
Net sea ice decrease	1.1+06	7.5e03	1.9e−04	−6.3e+07	7.9e03	1.8e−02

[a]Relative trend is trend divided by mean, except at the lower row where the numbers are the difference between the upper and lower rows (melting-growth).

5. Results

Results from the three NorESM1-M ensemble members are all investigated. For simplicity, the figures and tables only show results from the first member (except Figure 2), but conclusions are based on overall agreements between all ensemble members.

5.1. Mean State and Trends

Table 3 lists the mean change in sea ice mass (kg s^{-1}) exerted by the different freezing and melting processes as described in section 4. In the Barents Sea, bottom melting causes the highest change in sea ice mass, closely followed by congelation growth. Frazil growth and top melting are an order of magnitude smaller than the first two. In the Central Arctic Ocean, congelation growth is the process which contributes
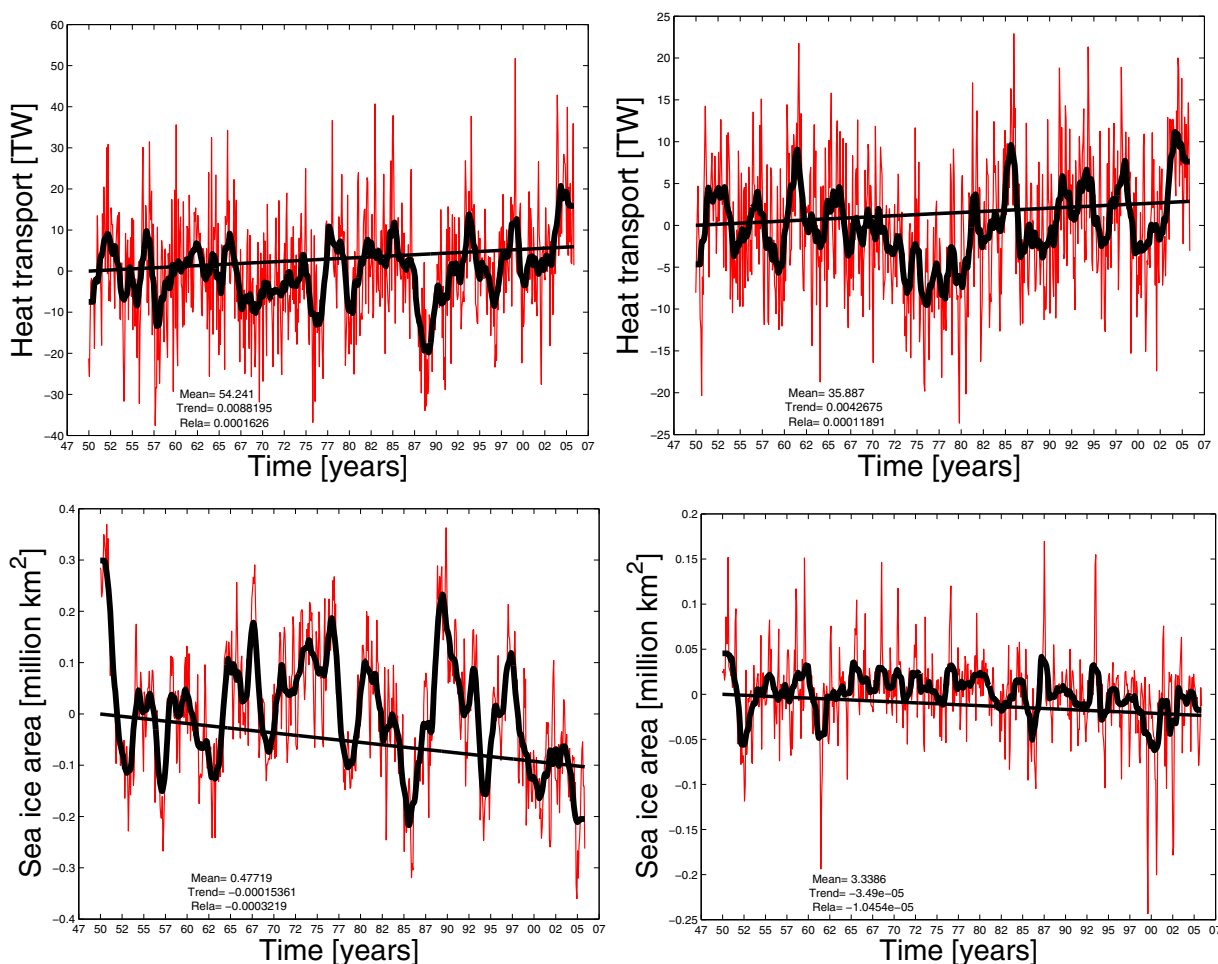

Figure 3. Time series of heat transport (TW) in (top left) BSO and (top right) FS, and sea ice area (million km^2) in the (bottom left) Barents Sea and (bottom right) Central Arctic Ocean. Note that the scales on the vertical axes are different.

Table 4. Peak Correlations and Lags Between Heat Transports in Different Gateways and Through Sea Surface (TW), and Sea Ice Area (m²) in the Barents Sea and Central Arctic Ocean[a]

	Opening	Correlation
Barents Sea	BSO	−0.41@−1
	FS	−0.26@0
	Surface	−0.27@−1
Central Arctic Ocean	BSO	−0.17@0
	FS	−0.24@0
	Surface	0.27@0

[a]Negative lags (in months) mean that sea ice area is lagging.

most to change in sea ice mass, with bottom melting and frazil growth as number two and three, respectively (Table 3). Also, a large part of the total bottom melting in the Central Arctic Ocean takes place in the relatively small shelf area north of Svalbard and east to Franz Josef Land (not shown) in the model.

Deseasoned time series for the heat transport through BSO and FS, and sea ice area in the Barents Sea and the Central Arctic Ocean are shown in Figure 3. The heat transports have positive trends, while the sea ice area trends are negative. The largest absolute heat transport trend is found in the BSO, but the BS has the largest relative trend, here defined as the trend divided by the mean (not shown). For sea ice area, the largest absolute and relative trends are both in the Barents Sea.

In the Central Arctic Ocean, both freezing and melting processes increase, but sea ice area decreases due to stronger melting than freezing (Table 3). The Barents Sea differs from this in that all freezing and melting processes decrease.

5.2. Variability in Time Series
Large interannual variability in the AW heat transport has shown to be important for the Barents Sea and Arctic sea ice extent [*Sandø et al.*, 2010; *Årthun et al.*, 2012; *Ivanov et al.*, 2012], but little is known about how this affects the sea ice processes discussed in section 4. Here correlations between time series are studied to detect possible relationships between ocean heat transport and sea ice area. Table 4 shows the correlations between heat transports in BSO and FS, and the sea ice area in the Barents Sea and the Central Arctic Ocean. From these correlations, it seems that the variability in the Barents Sea ice area is relatively strongly related to the BSO heat transport (−0.41@−1). The Central Arctic Ocean sea ice variability is somewhat connected to the net downward heat flux at the surface (0.27@0), and to the heat transport in the FS (−0.24@0). There are no significant correlations between the heat transports through the BS and the sea ice area in the Barents Sea or the Central Arctic Ocean. The same is true for the heat transports through the CN (not shown).

Table 5 shows correlations between the freezing and melting processes as described in section 4 and sea ice area. The highest correlation to sea ice area in the Barents Sea is with congelation growth (0.55@0), closely followed by bottom melting (0.51@0) (Table 5). Furthermore, Table 6 shows that the congelation growth in the Barents Sea is strongly correlated to the BSO heat transport (−0.41@0). The highest correlation to sea ice area in the Central Arctic Ocean is with bottom melting (0.56@0) (Table 5), which again is correlated to FS heat transport (0.22@2) (Table 6).

Considering the time lags in the highest correlations in Tables 4–6, sea ice area in the Barents Sea lags one month behind BSO heat transports (Table 4), which can partly be explained by the one month time lag between BSO heat transports and bottom melting in the Barents Sea (Table 6). Regarding the highest correlations in Table 5, these suggest that congelation growth and bottom melting affect the sea ice mass immediately in the Barents Sea and Central Arctic Ocean, respectively. Together with the spatial distributions of sea ice processes as presented in section 5.3, the results in this section are further analyzed and discussed in section 6.

Table 5. Peak Correlations and Lags Between Processes Changing Sea Ice Mass (kg s^{-1}) and Sea Ice Area (m²) in the Barents Sea and Central Arctic Ocean[a]

	Process	Correlation
Barents Sea	Bottom melting	0.51@0
	Top melting	0.22@1
	Congelation growth	0.55@0
	Frazil growth	0.37@−1
Central Arctic Ocean	Bottom melting	−0.56@0
	Top melting	−0.25@−13
	Congelation growth	−0.20@3
	Frazil growth	−0.23@1

[a]Negative lags (in months) mean that sea ice area is lagging.

Table 6. Peak Correlations and Lags Between Heat Transport (TW) Through the BSO (FS) and Processes Changing Sea Ice Mass (kg s^{-1}) in the Barents Sea and Central Arctic Ocean[a]

	Opening	Process	Correlation
Barents Sea	BSO	Bottom melting	−0.24@−1
		Top melting	
		Congelation growth	−0.41@0
		Frazil growth	−0.18@−8
Central Arctic Ocean	FS	Bottom melting	0.22@2
		Top melting	
		Congelation growth	
		Frazil growth	−0.18@−8

[a]Negative lags (in months) mean that sea ice processes are lagging.

5.3. Spatial Distribution of the Relationship Between Heat Transports, Freezing, Melting, and Sea Ice Area

Figure 4 presents correlations between BSO and FS heat transports, and bottom melting. Positive correlation reflects more melting as more heat is transported into the area. The resulting pattern for the BSO is one of positive correlations north of Svalbard and in the East Greenland Current where sea ice is assumed to be present all year round (Figure 1), and negative correlations in the West Spitsbergen Current and in the southern and central parts of the Barents Sea, which are only seasonally covered by sea ice. A similar pattern emerges for the FS heat transport, but here the negative correlations are more pronounced in the Greenland Sea. The reason for this similarity may be that the heat transports in the FS and BSO are positively correlated (0.53), so when the BSO heat transport is anomalously high, it will also be high in the FS. Furthermore, the area with significant positive correlations to bottom melting at the shelf north and east of Svalbard (Figure 4) coincide roughly with the area that contributes considerably to the total bottom melting in the Central Arctic Ocean. This suggests that the Svalbard branch of the West Spitsbergen Current is a "hot spot" in a double sense, where elevated levels of mixing due to strong tides are important for the cooling of the AW layer, for the regional heat budget, and the ice cover [*Sirevaag and Fer*, 2009]. Also, the study of *Ivanov et al.* [2012] indicates that heat flux from the ocean reduces the ice thickness in the AW inflow region east of Svalbard. The Svalbard branch also seems to have some influence on the northeastern Svalbard shelf at the entrance to the Barents Sea (Figure 4). The simulated net northward heat exchange between the Central Arctic Ocean and the Barents Sea is −14.3 TW, which means that heat is transported into the Barents Sea, most probably by AW entering the Barents Sea from the north [*Lind and Ingvaldsen*, 2012] and/or by Cold Bottom Water ($T < 0°C$) leaving through Barents Sea Exit [*Gammelsrød et al.*, 2009].

Likewise, correlations for congelation growth are shown in Figure 5. Negative correlations, whereby more heat transport is equivalent to less freezing, dominate the Arctic Ocean in both cases, while only BSO heat transport influences the whole Barents Sea. The largest correlations coincide roughly with areas of mean sea ice concentration less than 100%. Figure 6 shows the correlation between top and bottom melting, and sea ice area. This figure reveals that bottom melting has much stronger and wider influence than top melting on the sea ice area variability in the Arctic, as already shown by Table 5. The correlations patterns and the corresponding signs described in this section are discussed in section 6.

6. Discussion

Future changes in the Arctic sea ice area and its thickness represent one of the largest uncertainties in climate research [*Laxon et al.*, 2003]. In this study, the simulated sea ice area and its variability in the Barents Sea and Central Arctic Ocean were analyzed in terms of melting, freezing, and heat transport through the Arctic gateways.

6.1. Regional Differences in Impacts From Freezing and Melting on Sea Ice Area

Bottom melting is found to be most important for sea ice area variability in Central Arctic Ocean, while congelation growth shows highest correlations to sea ice area in the Barents Sea (Table 5). In addition, Figure 4 reveals some interesting results comprising both positive and negative correlations between heat transports and bottom melting in the Central Arctic Ocean and the Barents Sea, respectively. That more heat advected into an area should lead to more bottom melting as in the Central Arctic Ocean is not surprising, but more heat transport related to less bottom melting in the Barents Sea, as given by the negative correlations, necessitates further analysis. This can be explained by the sea ice concentration in the seasonally covered areas: more heat transported into these areas leads to less freezing by congelation growth (Figure 5, Table 6), and less ice is available to be melted. So therefore, more heat transport gives less congelation
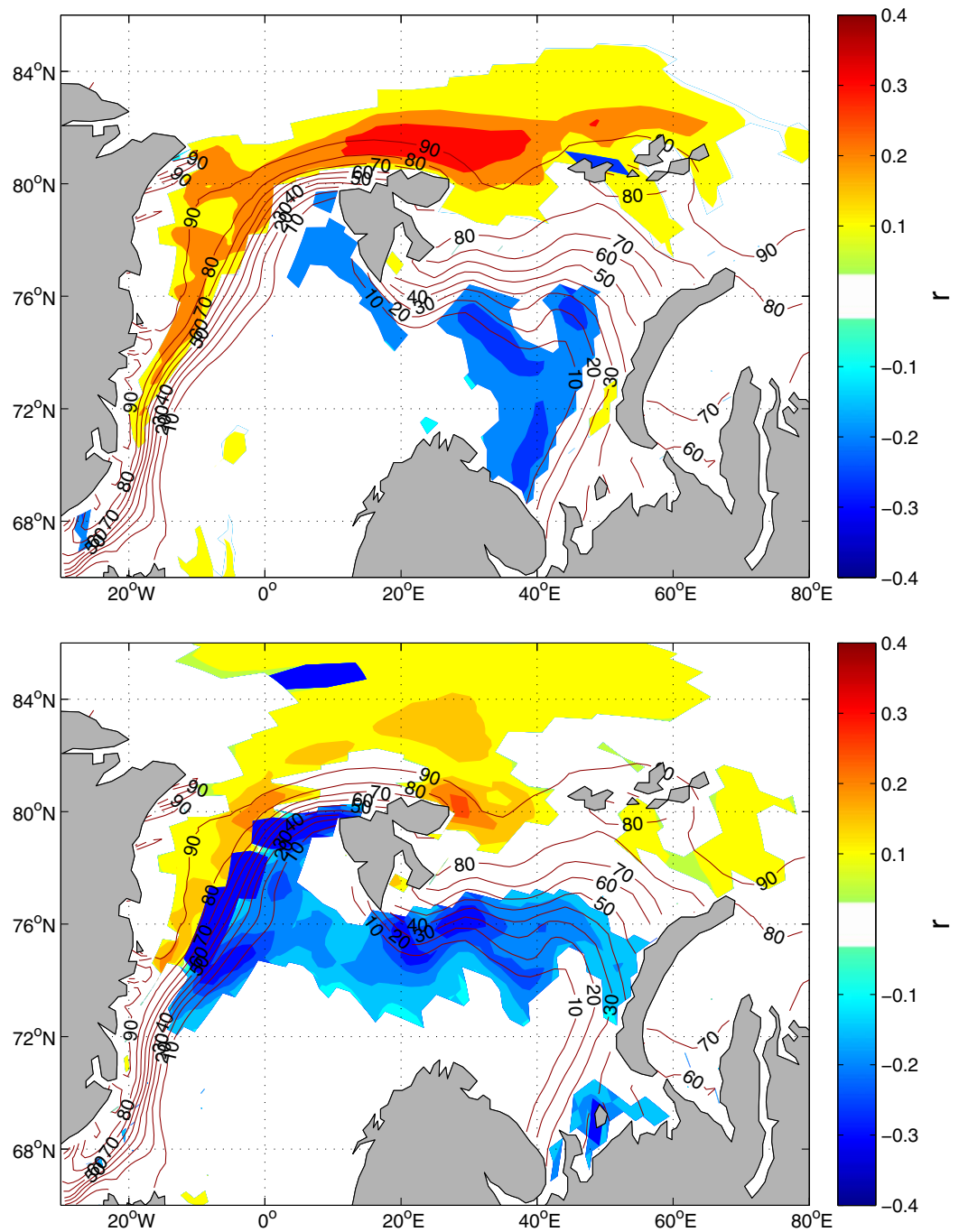
Figure 4. Significant correlations between linearly detrended (top) BSO and (bottom) FS heat transports (TW) and bottom melting (kg s^{-1}). Contours show mean sea ice concentration for the period 1950–2005.

growth and less sea ice, and finally less bottom melting. The order which these processes happen is supported by the lags between BSO heat transports, and the freezing and melting processes in Table 6: congelation growth responds immediately to heat transport through BSO, while bottom melting lags by one month.

This result is consistent with the statement in *Smedsrud et al.* [2013] that most of the ice loss in the Barents Sea ice during winter is not caused by ice that melted, but rather by ice that never formed. The same is not true for permanently ice covered regions like the Central Arctic Ocean
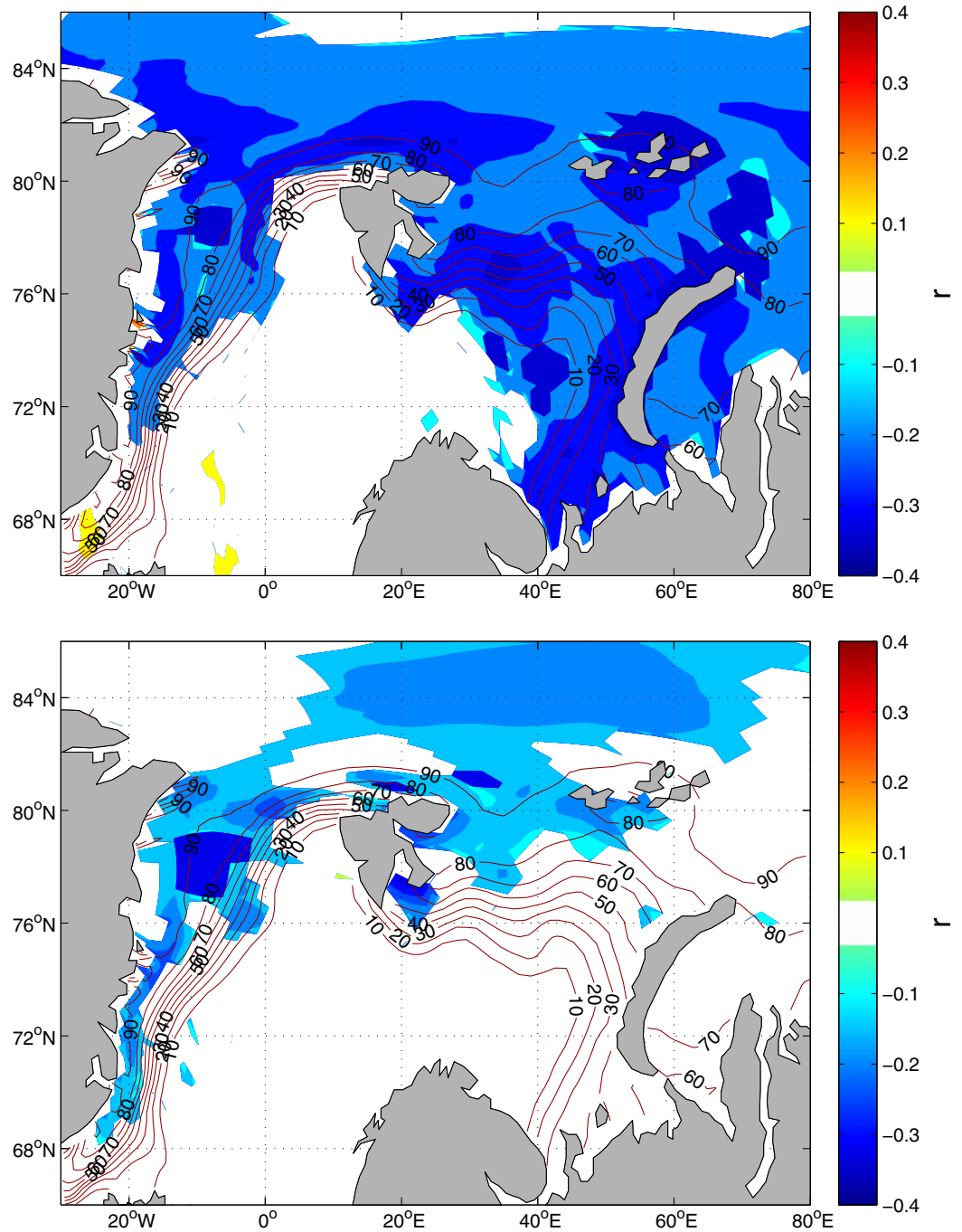
Figure 5. Significant correlations between detrended (top) BSO and (bottom) FS heat transports (TW) and congelation growth (kg s^{-1}). Contours show mean sea ice concentration for the period 1950–2005.

where sea ice is always available, and more FS heat transport leads to more melting. This is particularly true for the area northeast of Svalbard (Figure 4), where a large part of the total bottom melting takes place due to strong tides and upward mixing of AW [*Sirevaag and Fer*, 2009; *Ivanov et al.*, 2012]. It should be noted here that the heat transport through the FS also contain a component of southward flowing Polar Water which dilutes the northward flowing AW more in the FS than in the BSO where the southward component is relatively small [*Skagseth*, 2008]. This may explain some of the differences with respect to strength and area of correlation between BSO and FS in Figures 4 and 5.
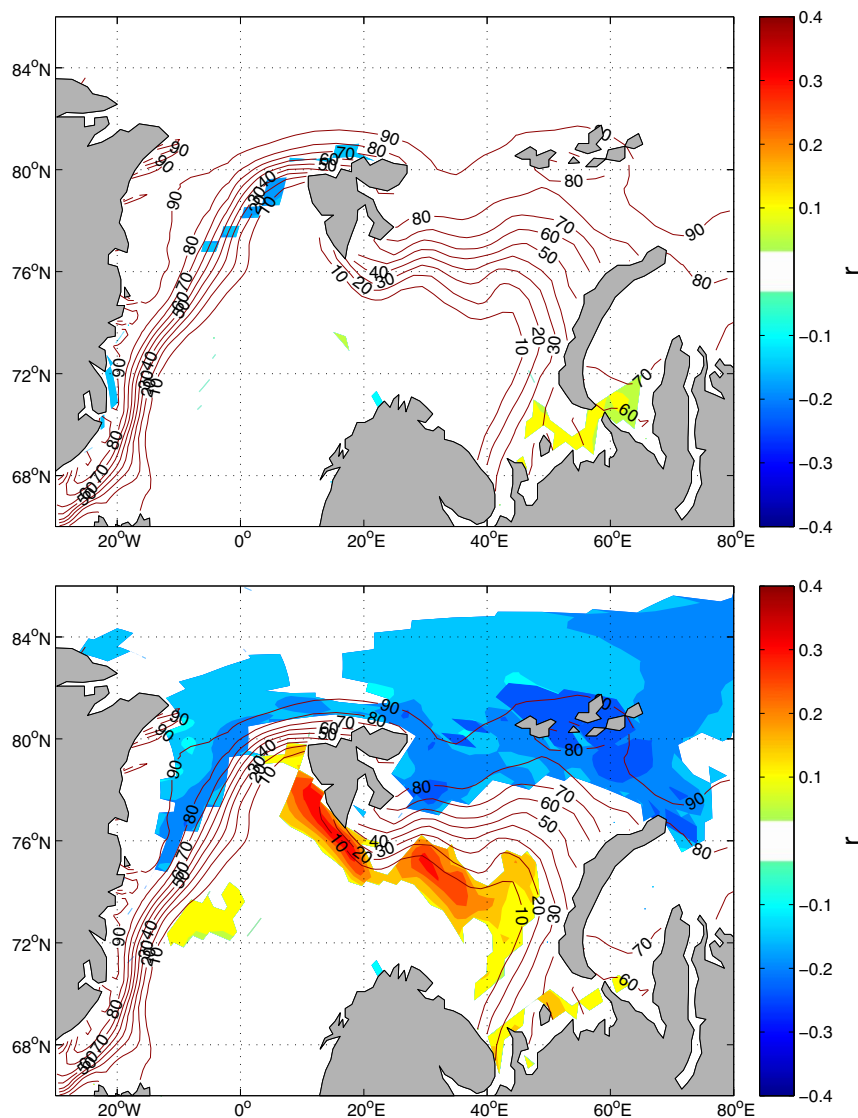
Figure 6. Significant correlations between detrended sea ice area (m²) and (upper) top and (lower) bottom melting (kg s⁻¹). Contours show mean sea ice concentration for the period 1950–2005.

The results from this study show that there is a difference between how much freezing and melting processes change sea ice area on average in the two regions, and how they influence the variability in the sea ice area. Bottom melting is the dominating process in changing sea ice area in the Barents Sea (Table 3), but congelation growth is most important for the variability (Table 5). For the Central Arctic Ocean, bottom melting is most important for the variability (Table 5) and congelation growth is most important for the mean sea ice area (Table 3).

6.2. Effects of a Changing Climate

Externally forced changes in the BSO heat transport will tend to be self-amplified through higher heat fluxes to the atmosphere, stronger outflow in the Barents Sea gateway and thereby stronger barotropic inflow through the BSO [*Smedsrud et al.*, 2013]. The deseasoned time series of sea ice area in Figure 3 show that there is a bigger negative absolute and relative trend in the Barents Sea than in the Arctic Ocean. This is consistent with results of *Årthun et al.* [2012] who found that the recent Arctic winter sea ice retreat was most pronounced in the Barents Sea, and may be consistent with a positive feedback loop as described by *Smedsrud et al.* [2013]. This study shows that the

SANDØ ET AL.   2105

reduction in sea ice area in the Barents Sea is first of all caused by a negative trend in congelation growth (Table 3) as a consequence of increased heat transports through the BSO (Table 6). It is well known that the AW looses most of its heat in the Barents Sea before entering the Arctic Ocean through the Barents Sea gateway [Pfirman et al., 1994]. Most of the Barents Sea ice cover usually forms during winter when surface heat loss cools the ocean to the freezing point, but in recent years, large areas of the Barents Sea has not formed sea ice [Smedsrud et al., 2013], mostly due to the recent high transport of AW [Årthun et al., 2012]. Therefore, in case of increased BSO heat transport, this study suggests that excess heat prevents ice formation, and shows that this is due to less congelation growth in the Barents Sea.

In the Central Arctic Ocean, the situation differs by both increased melting and ice formation, but the melting trend is bigger than the formation trend (Table 3), and the sea ice area decreases also here due to the dominance of stronger melting (Figure 3). Even though bottom melting is much strongly correlated to the sea ice area than top melting (Figure 6) and two orders of magnitude larger than top melting on average (Table 3), the bottom melting trend is only one order of magnitude larger, and the relative top melting trend is therefore the largest (Table 3). Therefore, while both the Barents Sea and Central Arctic Ocean ice areas seem to respond strongly to increased advection of heat in the ocean, the Central Arctic Ocean is also increasingly affected by top melting and a warming atmosphere. Higher Arctic air temperatures may be caused by an observed trend of more meridional flow over the Barents Sea region, which is associated with the Scandinavian blocking pattern [Smedsrud et al., 2013].

6.3. Implications for Model Development

Langehaug et al. [2013] reveal that NorESM1-M overestimates September sea ice area in the Barents Sea. This might be due to an underestimation of bottom melting and an overestimation of congelation growth, which both are closely related to the BSO heat transports. Like the other coupled climate models evaluated in this study, NorESM1-M also underestimates the BSO heat transport (Tables 1 and 2).

This study stresses the importance of heat transport in the ocean for the sea ice variability, and how the different processes involved in ice freezing and melting respond to this. It therefore emphasizes the need for realistic heat transports into the Arctic regions, both in terms of its mean and its variability, in order to get a proper sea ice area. Melsom et al. [2009] showed that heat transports into the Barents Sea were improved by oceanic downscaling and increased resolution. Therefore, higher resolution may improve sea ice area in global climate models, but precautions should be taken with regard to parameterizations of processes that depend on model resolution.

7. Summary and Conclusions

Three coupled climate models (CNRM-CM5, MRI-CGCM3, and NorESM1-M) have been evaluated against multiple estimates from the literature with respect to poleward ocean heat transport through four gateways to the Arctic. NorESM1-M transports are closest to the mean in both BSO and FS, the gateways which are closest to the regions of interest in this study (Figure 1), and were therefore chosen for further analysis.

The model results argue that increased heat transport in the BSO has strong influence on the ice formation in terms of reduced congelation growth ($r = -0.41@0$) and that this causes reduced sea ice area in the Barents Sea ($r = -0.41@-1$). BSO heat transport also affects the bottom melting in the Barents Sea ($-0.24@-1$), but increased heat transport does not yield increased bottom melting in this area. This can be explained by the total sea ice area available to be melted, which in case of increased heat transport through the BSO will be reduced due to less sea ice formation.

Freezing and melting processes are approximately balanced in the Barents Sea. This is not the case in the Central Arctic Ocean, where congelation growth strongly dominates the other processes in changing the sea ice mass, while bottom melting is more important for the variability of the sea ice area. There are negative trends in sea ice area in both the Barents Sea and the Central Arctic Ocean, but it is much bigger in the Barents Sea. This reflects the major trend in the BSO heat transport, which is more than twice as large as in any of the other gateways. Lastly, this study suggests that the ocean has stronger direct impact on changes

in sea ice mass in terms of freezing and melting than the atmosphere, both in the mean and with respect to variability.

References

Aagaard, K., and P. Greisman (1975), Toward new mass and heat budgets for the Arctic Ocean, *J. Geophys. Res.*, 80, 3821–3827.

Årthun, M., T. Eldevik, L. H. Smedsrud, Ø. Skagseth, and R. Ingvaldsen (2012), Quantifying the influence of Atlantic heat on Barents Sea ice variability and retreat, 25, 4736–4743.

Bekryaev, R. V., I. V. Polyakov, and V. A. Alexeev (2010), Role of polar amplification in long-term surface air temperature variations and modern Arctic warming, 23, 3888–3906.

Bentsen, M., et al. (2013), The Norwegian Earth System Model, NorESM1-M Part 1: Description and basic evaluation of the physical climate, *Geosci. Model Dev.*, 6, 687–720.

Boé, J., A. Hall, and X. Qu (2009), September sea-ice cover in the Arctic Ocean projected to vanish by 2100, *Nat. Geosci.*, 2, 341–343.

Chelton, D. B. (1983), Effects of sampling errors in statistical estimation, *Deep Sea Res., Part A*, 30(10), 1083–1103.

Comiso, J. C. (2012), Large decadal decline of the Arctic multiyear ice cover, *J. Clim.*, 25, 1176–1193.

Cuny, J., P. B. Rhinesand, and R. Kwok (2005), Davis Strait volume, freshwater and heat fluxes, *Deep Sea Res., Part I*, 52, 519–542.

Curry, B., C. M. Lee, and B. Petrie (2011), Volume, freshwater, and heat fluxes through Davis Strait, 2004–05, *J. Phys. Oceanogr.*, 41, 429–436.

Eldevik, T., and J. E. Ø. Nilsen (2013), The Arctic-Atlantic thermohaline circulation, *J. Clim.*, 26, 8698–8705.

Gammelsrød, T., Ø. Leikvin, V. Lien, W. P. Budgell, H. Loeng, and W. Maslowski (2009), Mass and heat transports in the NE Barents Sea: Observations and models, *J. Mar. Syst.*, 75, 56–69.

Harms, I. H., C. Schrum, and K. Hatten (2005), Numerical sensitivity studies on the variability of climate-relevant processes in the Barents Sea, *J. Geophys. Res.*, 110, C06002, doi:10.1029/2004JC002559.

Helland-Hansen, B., and F. Nansen (1909), The Norwegian Sea: Its Physical Oceanography Based Upon the Norwegian Researches 1900-1904, Report on Norwegian fish and marine investigations, 2, 2, 1–390.

Hopkins, T. S. (1991), The GIN Sea—A synthesis of its physical oceanography and literature review 1972–1985, *Earth Sci. Rev.*, 30, 175–319.

Hunke, E. C., and W. T. Lipscomb (2010), *CICE: the Los Alamos sea ice model documentation and software user's manual version 4.1*, Rep. LA-CC-06–012, T-3 Fluid Dyn. Group, Los Alamos Natl. Lab., Los Alamos, N. M.

Ingvaldsen, R. B., H. Loeng, and L. Asplin (2002), Variability in the Atlantic inflow to the Barents Sea based on a one-year time series from moored current meters, *Cont. Shelf Res.*, 22, 505–519.

Ingvaldsen, R. B., L. Asplin, and H. Loeng (2004), The seasonal cycle in the Atlantic transport to the Barents Sea during the years 1997–2001, *Cont. Shelf Res.*, 24, 1015–1032.

IPCC (2007), Global Climate Projections, in *Climate Change 2007*, edited by Solomon, S. et al., pp. 747–847, Cambridge Univ. Press, Cambridge, U. K.

Ivanov, V. V., V. A. Alexeev, I. Repina, N. V. Koldunov, and A. Smirnov (2012), Tracing Atlantic Water signature in the Arctic Sea ice cover east of Svalbard, *Adv. Meteorol.*, 2012, 1–11.

Kay, J. E., M. M. Holland, and A. Jahn (2011), Interannual to multidecadal Arctic sea ice extent trends in a warming world, *Geophys. Res. Lett.*, 38, L15708, doi:10.1029/2011GL048008.

Langehaug, H. R., F. Geyer, L. H. Smedsrud, and Y. Gao (2013), Arctic sea ice decline and ice export in the CMIP5 historical simulations, *Ocean. Modell.*, 71, 114–126.

Laxon, S., N. Peacock, and D. Smith (2003), High interannual variability of sea ice thickness in the Arctic region, *Nature*, 425, 947–950.

Lind, S., and R. B. Ingvaldsen (2012), Variability and impacts of Atlantic Water entering the Barents Sea from the north, *Deep Sea Res., Part I*, 62, 70–88.

Lindsay, R. W., and J. Zhang (2005), The thinning of Arctic Sea ice, 1988–2003: Have we passed a tipping point?, *J. Clim.*, 18, 4887–4893.

Loeng, H. (1991), Features of the physical oceanographic conditions of the Barents Sea, in *Proceedings of the Pro Mare Symposium on Polar Marine Ecology*, edited by C. C. E. Hopkins, E. Sakshaug, and N. A. Øritsland, pp. 5–18, Polar Research, Trondheim, Norway.

Maslowski, W., D. Marble, V. Walczowsli, U. Schauer, J. L. Clement, and A. J. Semtner (2004), On climatological mass, heat and salt transports through the Barents Sea and Fram Strait from a pan-Arctic coupled ice-ocean model simulation, *J. Geophys. Res.*, 109, C03032, doi: 10.1029/2001JC001039.

Melsom, A., V. S. Lien, and W. P. Budgell (2009), Using the Regional Ocean Modeling System (ROMS) to improve the ocean circulation from a GCM 20th century simulation, *Ocean Dyn.*, 59, 969–981.

Min, S.-K., X. Zhang., F. W. Zwiers, and T. Agnew (2008), Human influence on Arctic sea ice detectable from early 1990s, *Geophys. Res. Lett.*, 35, L21701, doi:10.1029/2008GL035725.

Mosby, H. (1962), Water, salt and heat balance of the north Polar Sea and the Norwegian Sea, *Geophys. Norv.*, 24, 289–313.

Overland, J. E., M. Wang, and S. Salo (2008), The recent Arctic warm period, *Tellus, Ser. A*, 60, 589–597.

Pfirman, S. L., D. Bauch, and T. Gammelsrød (1994), The Northern Barents Sea: Water mass distribution and modification, in *The Polar Oceans and their Role in Shaping the Global Environment*, edited by O. M. Johannessen, R. D. Muench, and J. E. Overland, pp. 77–94, AGU, Washington, D. C.

Polyakov, I. V., et al. (2010), Arctic Ocean warming contributes to reduced Polar ice cap, *J. Phys. Oceanogr.*, 40, 2743–2756.

Rudels, B. (1987), On the mass balance of the Polar Ocean with special emphasis on the Fram Strait, *Skr. Nor. Polarinst.*, 188, 1–53.

Sandø, A. B., J. E. Ø. Nilsen, Y. Gao, and K. Lohmann (2010), The importance of heat transports and local air-sea heat fluxes for the Barents Sea climate variability, *J. Geophys. Res.*, 115, C07013, doi:10.1029/2009JC005884.

Sandø, A. B., A. Melsom, and P. W. Budgell (2014), Downscaling IPCC control and future scenario with focus on the Barents Sea, *Ocean Dyn*, in press.

Santer, B. D., et al. (2008), Consistency of modelled and observed temperature trends in the tropical troposphere, *Int. J. Climatol.*, 28, 1703–1722.

Schauer, U., A. Beszczynska-Moller, W. Walcowski, E. Fachbach, J. Piechura, and E. Hansen (2008), Variation of measured heat flow through the Fram Strait between 1997 and 2006, in *Arctic—Subarctic Ocean Fluxes (ASOF)*, edited by R. R. Dickson, J. Meincke, and P. Rhines, pp. 65–85, Springer, Dordrecht, Netherlands.

Serreze, M., and J. A. Francis (2006), The Arctic on the fast track of change, *Weather*, 61, 65–69.

Serreze, M. C., M. M. Holland, and J. Stroeve (2007), Perspectives on the Arctic's shrinking sea-ice cover, *Science*, 315, 1533–1536.

Sirevaag, A., and I. Fer (2009), Early spring oceanic heat fluxes and mixing observed from drift stations north of Svalbard, *J. Phys. Oceanogr.*, 39, 3049–3069.

SANDØ ET AL.   2107

Skagseth, Ø. (2008), Recirculation of Atlantic Water in the western Barents Sea, *Geophys. Res. Lett.*, *35*, L11606, doi:10.1029/2008GL033785.

Skagseth, Ø., T. Furevik, R. Ingvaldsen, H. Loeng, K. A. Mork, K. A. Orvik, and V. Ozhigin (2008), Volume and heat transports to the Arctic Ocean via the Norwegian and Barents Seas, in *Arctic—Subarctic Ocean Fluxes (ASOF)*, edited by R. R. Dickson, J. Meincke, and P. Rhines, pp. 1–29, Springer.

Skagseth, Ø., K. F. Drinkwater, and E. Terrile (2011), Wind-induced transport of the Norwegian Coastal Current in the Barents Sea, *J. Geophys. Res.*, *116*, C08007, doi:10.1029/2011JC006996.

Smedsrud, L. H., R. Ingvaldsen, J. E. Ø. Nilsen, and Ø. Skagseth (2010), Heat in the Barents Sea: Transport, storage, and surface fluxes, *Ocean Sci.*, *6*, 219–234.

Smedsrud, L., et al., (2013), The role of the Barents Sea in the Arctic climate system, *Rev. Geophys.*, *51*, 415–449, doi:10.1002/rog.20017.

Stroeve, J., M. M. Holland, W. Meier, T. Scambos, and M. Serreze (2007), Arctic sea ice decline: Faster than forecast, *Geophys. Res. Lett.*, *34*, L09501, doi:10.1029/2007GL029703.

Stroeve, J., V. Kattsov, A. Barrett, M. Serreze, T. Pavlova, M. Holland, and W. N. Meier (2012), Trends in Arctic sea ice extent from CMIP5, CMIP3 and observations, *Geophys. Res. Lett.*, *39*, L16502, doi:10.1029/2012GL052676.

Taylor, K. E. (2001), Summarizing multiple aspects of model performance in a single diagram, *J. Geophys. Res.*, *106*, 7183–7192.

Taylor, K. E., R. J. Stouffer, and G. A. Meehl (2012), An overview if CMIP5 and the experiment design, *Bull. Am. Meteorol. Soc.*, *93*, 485–498.

Tsubouchi, T., et al., (2012) The Arctic Ocean in summer: A quasi-synoptic inverse estimate of boundary fluxes and water mass transformation, *J. Geophys. Res.*, *117*, C01024, doi:10.1029/2011JC007174.

Voldoire, A., et al. (2011), The CNRM-CM5.1 global climate model: Description and basic evaluation, *Clim Dyn.*, *40*, 2091–2121.

Vowinkel, E., and S. Orvig (1970), The climate of the North Pole basin, in *World Survey of Climatology*, edited by S. Orvig, pp. 129–252, Elsevier, New York.

Yukimoto, S., et al. (2012), A new global climate model of the Meteorological Research Institute: MRI-CGCM3—Model description and basic performance, *J. Meteorol. Soc. Jpn.*, *90A*, 23–64.

Zhang, X., and J. Zhang (2001), Heat and freshwater budgets and pathways in the Arctic Mediterranean in a coupled ocean/sea-ice model, *J. Oceanogr.*, *57*, 207–234.